Distortions produced in optical homodyne tomography

Filippus S. Roux ●*

National Metrology Institute of South Africa, Meiring Naudé Road, Brummeria 0040, Pretoria, South Africa

An analysis of the homodyne tomography process that is often used to determine the Wigner functions of quantum optical states is performed to consider the effects of the spatiotemporal degrees of freedom. The homodyne tomography process removes those parts of the input state that are not associated with the mode of the local oscillator by tracing out those degrees of freedom. Using a functional approach to incorporate all the spatiotemporal degrees of freedom, we find that this reduction in the degrees of freedom introduces distortions in the observed Wigner function. The analysis also shows how the homodyne tomography process introduces a scaling caused by the efficiency and a resolution that depends on the strength of the local oscillator. As examples, we consider coherent states, Fock states, and squeezed vacuum states.

I. INTRODUCTION

Homodyne tomography [1] is widely used to determine the Wigner functions of quantum optical states in terms of their particle-number degrees of freedom, pertaining to specific spatiotemporal modes. It has been used to measure the Wigner functions of squeezed vacuum states [2,3], Fock states [4–6], photon added states [7,8], Schrödinger cat states [9,10], and many others. The quality of specially prepared quantum states that are used as resources in quantum information systems can be determined with homodyne tomography. However, it begs the question of the quality of the homodyne tomography process itself.

Various aspects of the homodyne tomography process have been investigated [11–13], including the temporal effects [14] and the efficiency and noise of detector systems [15,16]. Mathematical and statistical methods with which Wigner functions are constructed from the measured data have been improved significantly over time.

These analyses generally assume that the measurements from which the Wigner functions of quantum states are constructed are restricted to the part of the Hilbert space associated with the mode of the local oscillator, and the part of the state not associated with this mode is represented as a loss. In free space, a quantum optical state contains an infinite number of spatiotemporal degrees of freedom in addition to its particle-number degrees of freedom. It is not possible to measure all these degrees of freedom in a tomography process. Some form of dimensional reduction is inevitable in any such measurement process. Homodyne tomography imposes this dimensional reduction primarily through an overlap by the mode of the local oscillator, but the detector system can also have an effect on the dimensional reduction process. All the unobserved degrees of freedom of the state are traced out.

Here, the intrinsic fidelity of the homodyne tomography process is investigated. To avoid making any assumptions about the spatiotemporal degrees of freedom in the process, we use a Wigner functional approach [17–20]. It allows us to incorporate all the spatiotemporal degrees of freedom in the analysis. We find that this careful consideration of the effects of the spatiotemporal degrees of freedom reveals a more detailed picture of the process, going beyond the existing understanding [1]. The main reason for the Wigner functional approach is to be able to investigate the effect of all the spatiotemporal degrees of freedom, which is not in general possible with previous approaches. The Wigner functional approach is extremely powerful in that it does not impose any limitations on the modeling of the physical system. Previous approaches always impose such limitations because they are based on a finite number of known modes, which are often notoriously difficult to determine. Although there are several scenarios where a finite number of known modes can provide an adequate analysis, there are also several cases where it does not. In the case of homodyne tomography where a state (such as a general squeezed state) cannot be parametrized in terms of a finite number of known modes, the Wigner functional approach is necessary for a successful analysis. Even in cases where states can be parametrized in terms a single mode (such as the coherent state and the single-mode Fock states), the Wigner functional approach reveals effects that have not been revealed by previous analyses. We selected the set of examples that we analyze to reveal these new effects, but we also show that, under suitable conditions, they reproduce previous results.

While our formulation of the homodyne tomography process provides the general procedure that can be applied to investigate the spatiotemporal effects in any homodyne tomography application, the derivation and the examples that we consider already reveal salient features of the process. These features include the appearance of an artifact at the origin of the functional phase space unless single-mode detection is employed; a scaling of the observed Wigner function caused by the quantum efficiency of the detectors; and a finite resolution for the rendering of the observed Wigner function. Although it is known that the Wigner functions obtained from
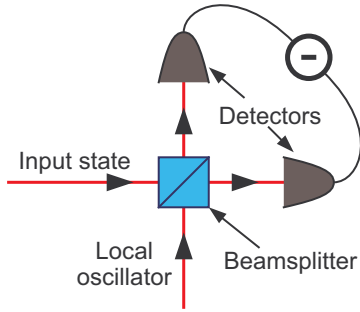
---

*froux@nmisa.org

FIG. 1. Diagram of the homodyne tomography system.

homodyne tomography can be distorted versions of the input states, the mechanism for such distortions is generally attributed to the loss of purity caused by losses in the system [1]. Here we reveal the exact nature of the process and show that the observed Wigner function can be rendered as a mixed state even without losses in the process. For example, while a coherent state remains pure despite losses, we show that the observed Wigner function is rendered as a mixed state under certain conditions.

In this analysis, we make extensive use of generating functions [21]. Such generating functions are employed to represent the distributions obtained from the homodyne detection process, and also for the Fock states that are considered in one of the examples. The expressions of these generating functions are derived in the Appendix.

II. OPTICAL HOMODYNING

There are different versions of the homodyning system that has been developed since its inception (see Ref. [1] and references therein). They include heterodyning and double homodyning systems [22,23]. However, we consider the basic homodyning system here, as depicted in Fig. 1. The local oscillator is a coherent state with a mode that is parametrized in terms of a spectral function. The input state is mixed with the local oscillator via a 50:50 beam splitter. The light from both output ports of the beam splitter is sent to identical detectors. The intensities registered by these detectors are subtracted from each other and then binned to provide a photon number probability distribution.

A. Wigner functionals

Formally, we represent the quantum optical state on which the homodyne tomography process is applied in terms of all its degrees of freedom by using a Wigner functional $W[\alpha]$ [17–20]. Such Wigner functionals are defined on a functional phase space where $\alpha(\mathbf{k})$ is the functional's field variable (itself a spectral function of the wave vector $\mathbf{k}$). For example, the Wigner functional of a coherent state is given by

$$W_{\mathrm{coh}}[\alpha] = \mathcal{N}_0 \exp(-2\|\alpha - \varphi\|^2), \tag{1}$$

where $\alpha(\mathbf{k})$ is the field variable and $\varphi(\mathbf{k})$ is the parameter function. For a pure Gaussian state such as the coherent state, the normalization constant is given by $\mathcal{N}_0 = 2^\Omega$, where Ω is a divergent cardinal number representing the infinite number of dimensions (or degrees of freedom) of the functional phase

space. The magnitude of the field variables (or parameter functions) in the exponent is given by

$$\|\alpha\|^2 = \int \alpha^*(\mathbf{k})\alpha(\mathbf{k})\frac{d^3k}{(2\pi)^3} \equiv \alpha^* \diamond \alpha. \tag{2}$$

To alleviate the complexity of the expressions that are obtained in this analysis, we introduce a $\diamond$ contraction to represent the integral over wave vectors shared by two functions. Such contractions can also involve kernel functions. For example

$$\alpha^* \diamond K \diamond \alpha \equiv \int \alpha^*(\mathbf{k})K(\mathbf{k}, \mathbf{k}')\alpha(\mathbf{k}')\frac{d^3k}{(2\pi)^3}\frac{d^3k'}{(2\pi)^3}, \tag{3}$$

where $K(\mathbf{k}, \mathbf{k}')$ is the kernel. Since we focus on the spatiotemporal degrees of freedom in this analysis, these $\diamond$ contractions only involve the integration over wave vectors, ignoring the polarization degrees of freedom. However, the analysis can be readily generalized to incorporate the polarization degrees of freedom.

At times, we perform functional integrations over Wigner functionals or products of Wigner functionals. Such functional integrations are represented with a functional integration measure. For example, the trace of the coherent state, which is obtained from the functional integration of its Wigner functional, is represented by

$$\int W_{\mathrm{coh}}[\alpha]\mathcal{D}^\circ[\alpha] = 1. \tag{4}$$

The functional integration measure $\mathcal{D}^\circ[\alpha]$ includes a factor of $1/2\pi$ for every degree of freedom.

The homodyne tomography process causes the reduction of the Wigner functional to a Wigner *function* $W(\alpha_0)$, where α_0 is a complex variable defined on a two-dimensional subspace of the infinite-dimensional functional phase space. It requires that all the discarded degrees of freedom be traced out.

Naively, this reduction process implies that the field variable of the Wigner functional is replace by $\alpha(\mathbf{k}) \to \alpha_0\Gamma(\mathbf{k})$ where $\Gamma(\mathbf{k})$ is the normalized mode of the local oscillator, represented as an angular spectrum, and that all the other degrees of freedom are simply discarded by the trace process. It turns out that the actual dimensional reduction process associated with homodyne tomography is in general more complicated than this naive view.

B. Cross-correlation function

When homodyning measurements are used to perform quantum state tomography, it is necessary to measure the photon-number statistics of the difference in intensity. Instead of the number operator measuring the average intensity, we need to use the projection operators for n photons for the analysis. Separate projection operators are used for the respective detectors, leading to two separate photon-number distributions for the two detectors. The difference between the measurements corresponds to the convolution of the distribution at one detector with the mirror image of the distribution at the other detector, which is the same as the cross-correlation function of the two distributions.

Assume that $P_1(n)$ and $P_2(n)$ represent the probability distributions for detecting photons at the two respective

detectors. The cross-correlation of the two distributions is then given by

$$R(m) = \sum_{n=0}^{\infty} P_1(n)P_2(n+m), \tag{5}$$

where m can be any signed integer. The requirement that $n + m > 0$ is maintained by the distributions themselves, being zero for negative arguments. A generating function for $R(m)$ is obtained by multiplying it by K^m, where K is the generating parameter and summing over m:

$$\mathcal{R}(K) = \sum_{m=-\infty}^{\infty} K^m R(m) = \sum_{n=0}^{\infty} \sum_{m=-\infty}^{\infty} K^m P_1(n)P_2(n+m). \tag{6}$$

Then we redefine $m \rightarrow p - n$ to get

$$\mathcal{R}(K) = \sum_{n,p=0}^{\infty} K^{p-n} P_1(n)P_2(p) = \mathcal{P}_1(K)\mathcal{P}_2(K^{-1}), \tag{7}$$

where we enforced the positivity of both arguments to obtain summations that start from 0, and where we introduced the generating functions for the original distributions, given by

$$\mathcal{P}_1(K) = \sum_{n=0}^{\infty} K^n P_1(n), \quad \mathcal{P}_2(K) = \sum_{n=0}^{\infty} K^n P_2(n). \tag{8}$$

As such, the generating function in Eq. (7) for the cross-correlation of the two distributions is given in terms of the generating functions of the respective distributions.

Here, we treated $P_1(n)$ and $P_2(n)$ as being statistically independent distributions. However, they are measured at the same time and the correlation is based on these simultaneous measurements. Therefore, the cross-correlation should be represented as a combined operator that is traced with the state to determine the cross-correlated distribution. Based on Eq. (7), a generating function for such operators is of the form

$$\hat{\mathcal{R}}(K) = \sum_{n=0}^{\infty} \sum_{p=0}^{\infty} K^{p-n} \hat{P}_n^{(1)} \hat{P}_p^{(2)} = \hat{\mathcal{P}}_1(K)\hat{\mathcal{P}}_2(K^{-1}), \tag{9}$$

where $\hat{P}_n^{(1)}$ and $\hat{P}_n^{(2)}$ are the n-photon projection operators associated with the respective detectors and $\hat{\mathcal{P}}_1(K)$ and $\hat{\mathcal{P}}_2(K)$ are their respective generating functions.

C. Detectors

The derivation of the generating function for the Wigner functionals of the n-photon projection operators [Eq. (A11)] is provided in the Appendix. We use two such generating functions with identical detector kernels D (they need to be identical for successful homodyning) to represent the two photon-number resolving detectors in the homodyning system. These generating functions are combined as in Eq. (9). The Wigner functional of the resulting combined generating function is

$$\mathcal{W}_{\hat{R}} = \mathcal{M}_K \exp[-2\mathcal{J}_K(\alpha^* \diamond D \diamond \alpha - \beta^* \diamond D \diamond \beta)], \tag{10}$$

where $\alpha(\mathbf{k})$ and $\beta(\mathbf{k})$ are the field variables associated with the respective detectors, and

$$\mathcal{M}_K = \frac{(4K)^{\mathrm{tr}\{D\}}}{(1+K)^{2\mathrm{tr}\{D\}}}, \quad \mathcal{J}_K = \frac{1-K}{1+K}, \tag{11}$$

for K being the generating parameter.

Here, we use W to represent Wigner functionals and $\mathcal{W}$ to represent generating functions of Wigner functionals. Generating functions for other quantities or functions that are not Wigner functionals are represented by other letters such as $\mathcal{P}$ or $\mathcal{R}$.

D. Beam splitter

The cross-correlation operator in Eq. (9) is traced with the state that is obtained after the beam splitter. The measurements can therefore be represented by

$$\langle \hat{R} \rangle = \mathrm{tr}\{\hat{U}_{\mathrm{BS}}(\hat{\rho}_{\mathrm{in}} \otimes \hat{\rho}_{\mathrm{lo}})\hat{U}_{\mathrm{BS}}^\dagger \hat{R}\}, \tag{12}$$

where $\hat{\rho}_{\mathrm{in}}$ and $\hat{\rho}_{\mathrm{lo}}$ are the density operators for the input state and the local oscillator, respectively, and $\hat{U}_{\mathrm{BS}}$ is the unitary operator for the beam splitter. Combined with the beam splitter's unitary operators, the detection operator becomes

$$\hat{R}' = \hat{U}_{\mathrm{BS}}^\dagger \hat{R} \hat{U}_{\mathrm{BS}}. \tag{13}$$

The unitary transformation for a 50 : 50 beam splitter applied to the Wigner functional of a state is represented by a transformation of the field variables in the argument of the Wigner functional, given by

$$\alpha(\mathbf{k}) \rightarrow \frac{1}{\sqrt{2}}[\alpha(\mathbf{k}) + i\beta(\mathbf{k})],$$

$$\beta(\mathbf{k}) \rightarrow \frac{1}{\sqrt{2}}[\beta(\mathbf{k}) + i\alpha(\mathbf{k})]. \tag{14}$$

However, since the unitary operators appear in the opposite order in Eq. (13), we need to apply the inverse transformations to the Wigner functional in Eq. (10), and thereby obtain

$$\mathcal{W}_{\hat{R}}' = \mathcal{M}_K \exp[i2\mathcal{J}_K(\beta^* \diamond D \diamond \alpha - \alpha^* \diamond D \diamond \beta)]. \tag{15}$$

E. Local oscillator

The generating function in Eq. (15) is multiplied with the Wigner functional for the local oscillator before the beam splitter and traced over the local oscillator's degrees of freedom. The resulting operator is represented as

$$\hat{H} = \mathrm{tr}_{\mathrm{lo}}\{\hat{\rho}_{\mathrm{lo}} \hat{U}_{\mathrm{BS}}^\dagger \hat{R} \hat{U}_{\mathrm{BS}}\}. \tag{16}$$

In terms of the Wigner functionals, the trace is performed by evaluating the functional integration over β, which is the field variable associated with the local oscillator. The trace produces the Wigner functional of the operator that is used to produce the distribution obtained from the homodyne process. It reads

$$\mathcal{W}_{\hat{H}}[\alpha](K) = \int W_{\mathrm{lo}}[\beta] \mathcal{W}_{\hat{R}}'[\alpha, \beta] \mathcal{D}^\circ[\beta]$$

$$= \mathcal{M}_K \exp\big[i2\mathcal{J}_K(\gamma^* \diamond D \diamond \alpha - \alpha^* \diamond D \diamond \gamma)$$

$$+ 2\mathcal{J}_K^2 \alpha^* \diamond D \diamond \alpha\big], \tag{17}$$

where $W_{\text{lo}}[\beta]$ is the Wigner functional for the coherent state of the local oscillator, and $\gamma(\mathbf{k})$ is the angular spectrum of the parameter function (mode function) that parametrized the state of the local oscillator.

The exponent in Eq. (17) contains the terms that combine into the contraction of the local oscillator mode with a real valued field variable (the quadrature variable) along a direction determined by the phase of the local oscillator mode. The exponent also contains a term that is independent of the local oscillator mode, and which is responsible for some of the distortions.

III. PROBABILITY DISTRIBUTION

The generating function for the distribution produced by the homodyning process is obtained by multiplying the Wigner functional of the state $W[\alpha]$ by Eq. (17) and computing the trace of the product. The resulting generating function for the cross-correlation distribution is

$$\mathcal{R}(K) = \sum_{m=-\infty}^{\infty} K^m R(m) = \int W[\alpha] \mathcal{W}_{\hat{H}}[\alpha](K) \mathcal{D}^{\circ}[\alpha], \quad (18)$$

where $R(m)$ is the probability distribution for the cross-correlation. It is not a functional anymore because all the field variables have been integrated out.

Following the inverse Radon transform approach [2] to obtain the observed Wigner function from the homodyning experimental results, we need to extract the probability distribution. Since the index m also runs over negative integers, we cannot extract individual terms with the aid of derivatives, as is often done with generating functions. Instead, the individual probabilities are extracted with an auxiliary integral for the Kronecker delta $\delta_{m,n}$:

$$\frac{1}{2\pi} \int_{-\pi}^{\pi} \exp[i(m-n)\phi] d\phi = \delta_{m,n}. \quad (19)$$

It implies that the probability distribution for the cross-correlation is extracted from its generating function by

$$R(n) = \sum_{m=-\infty}^{\infty} R(m) \frac{1}{2\pi} \int_{-\pi}^{\pi} \exp[i(m-n)\phi] d\phi$$
$$= \frac{1}{2\pi} \int_{-\pi}^{\pi} \exp(-in\phi) \mathcal{R}(e^{i\phi}) d\phi. \quad (20)$$

The expression in Eq. (17) is substitute into Eq. (18), which is then substituted into Eq. (20). When we replace $K = \exp(i\phi)$ in $\mathcal{J}_K$ and $\mathcal{M}_K$, they become

$$\mathcal{J}_K \to -i \tan\left(\frac{1}{2}\phi\right), \quad \mathcal{M}_K \to \frac{1}{\cos^{2\text{tr}\{D\}}\left(\frac{1}{2}\phi\right)}. \quad (21)$$

The expression for the distribution thus becomes

$$R(n) = \frac{1}{2\pi} \int_{-\pi}^{\pi} \frac{\exp(-in\phi)}{\cos^{2\text{tr}\{D\}}\left(\frac{1}{2}\phi\right)} \int W[\alpha]$$
$$\times \exp\left[2 \tan\left(\frac{1}{2}\phi\right)(\gamma^* \diamond D \diamond \alpha - \alpha^* \diamond D \diamond \gamma)\right.$$
$$\left. - 2 \tan^2\left(\frac{1}{2}\phi\right)\alpha^* \diamond D \diamond \alpha\right] \mathcal{D}^{\circ}[\alpha] d\phi. \quad (22)$$

For convenience, the parameter function of the local oscillator is represented as $\gamma(\mathbf{k}) = \gamma_0 \exp(i\theta)\Gamma(\mathbf{k})$, where

$$\gamma_0 \equiv \|\gamma\| = \sqrt{\gamma^* \diamond \gamma}, \quad (23)$$

is the magnitude of the parameter function, $\Gamma(\mathbf{k})$ is a normalized spectral function, so that $\|\Gamma\| = 1$, and θ is a variable phase. The distribution is now treated as a function of a continuous variable x. We define

$$x = n\Delta x = \frac{n}{\gamma_0}, \quad (24)$$

where we use the inverse of the magnitude of the local oscillator mode function to represent the small increment $\Delta x = \gamma_0^{-1}$. The distribution then becomes

$$R(x, \theta) = \frac{1}{2\pi} \int_{-\pi}^{\pi} \frac{\exp(-ix\gamma_0\phi)}{\cos^{2\text{tr}\{D\}}\left(\frac{1}{2}\phi\right)} \int W[\alpha]$$
$$\times \exp\left[2 \tan\left(\frac{1}{2}\phi\right)(\gamma^* \diamond D \diamond \alpha - \alpha^* \diamond D \diamond \gamma)\right.$$
$$\left. - 2 \tan^2\left(\frac{1}{2}\phi\right)\alpha^* \diamond D \diamond \alpha\right] \mathcal{D}^{\circ}[\alpha] d\phi, \quad (25)$$

where we show the probability distribution's dependence on the phase of the local oscillator θ.

IV. OBSERVED WIGNER FUNCTION

To recover the *observed* Wigner function from the measured probability distribution, we perform two steps that implement the inverse Radon transform. The probability distribution in terms of x is interpreted as a marginal distribution obtained from the partial integration of the Wigner functional, retaining only a one-dimensional variation along a direction determined by θ and Γ. The result is a function and not a functional. In the first step, this marginal distribution is converted into a corresponding slice of the associated characteristic function $\chi(r, \theta)$ via a Fourier transform

$$\chi(r, \theta) = \int R(x, \theta) \exp(ixr) dx, \quad (26)$$

where r and θ are treated as cylindrical coordinates, but with ranges given by $-\infty < r < \infty$ and $0 \leqslant \theta \leqslant \pi$. When we substitute Eq. (25) into Eq. (26) and evaluate the integral over x, it produces a Dirac δ function

$$\int \exp(-ix\gamma_0\phi) \exp(ixr) dx = 2\pi\delta(\gamma_0\phi - r). \quad (27)$$

The integration over ϕ therefore replaces

$$\phi \to \frac{r}{\gamma_0} = r\Delta x. \quad (28)$$

Hence, it imposes a boundary on the characteristic function. Since $-\pi < \phi < \pi$, it follows that $-\pi\gamma_0 < r < \pi\gamma_0$. Provided that the characteristic function lies within this region, we can ignore the boundary. Otherwise the characteristic function would be clipped by the boundary. We assume that γ_0 is large enough that the characteristic function is contained inside this boundary.

In the second step, a symplectic Fourier transform is applied to the characteristic function to produce the observed

Wigner function as a function of q and p. It reads

$$W'(q, p) = \frac{1}{2\pi} \int \chi(\xi, \zeta) \exp(iq\xi - ip\zeta) d\zeta \, d\xi, \quad (29)$$

where ξ and ζ are Cartesian coordinates, associated with the cylindrical coordinates r and θ, such that

$$r^2 = \tfrac{1}{2}(\zeta^2 + \xi^2). \quad (30)$$

The integrations over x and ϕ in Eq. (26) and Eq. (25) then lead to

$$W'(q, p) = \mathcal{N} \int \frac{W[\alpha]}{\cos^{2\mathrm{tr}\{D\}}\left(\frac{1}{2}r\Delta x\right)}$$

$$\times \exp\left[-2\tan^2\left(\frac{1}{2}r\Delta x\right)\alpha^* \diamond D \diamond \alpha \right.$$

$$+ 2\tan\left(\frac{1}{2}r\Delta x\right)(\gamma^* \diamond D \diamond \alpha - \alpha^* \diamond D \diamond \gamma)$$

$$\left. + iq\xi - ip\zeta \right]\mathcal{D}^\circ[\alpha] d\zeta \, d\xi, \quad (31)$$

where we introduce a normalization constant $\mathcal{N}$. For large enough γ_0 (small enough Δx),

$$\tan\left(\tfrac{1}{2}r\Delta x\right) = \tfrac{1}{2}r\Delta x + O(r^3\Delta x^3),$$

$$\cos\left(\tfrac{1}{2}r\Delta x\right) = 1 + O(r^2\Delta x^2). \quad (32)$$

If the characteristic function has a small enough size compared with the boundary, we can represent the observed Wigner function as

$$W'(q, p) = \mathcal{N} \int W[\alpha] \exp\left[-\frac{1}{2}r^2\Delta x^2 \alpha^* \diamond D \diamond \alpha \right.$$

$$+ r\Delta x(\gamma^* \diamond D \diamond \alpha - \alpha^* \diamond D \diamond \gamma)$$

$$\left. + iq\xi - ip\zeta \right]\mathcal{D}^\circ[\alpha] d\zeta \, d\xi$$

$$= \mathcal{N} \int W[\alpha] \exp\left[-\frac{1}{4}(\zeta^2 + \xi^2)\Delta x^2 \alpha^* \diamond D \diamond \alpha \right.$$

$$+ \frac{1}{\sqrt{2}}(\zeta - i\xi)\Gamma^* \diamond D \diamond \alpha$$

$$- \frac{1}{\sqrt{2}}(\zeta + i\xi)\alpha^* \diamond D \diamond \Gamma$$

$$\left. + iq\xi - ip\zeta \right]\mathcal{D}^\circ[\alpha] d\zeta \, d\xi, \quad (33)$$

where we converted r, together with θ from within γ, into ζ and ξ in the last expression.

Without the second-order term in the exponent, the integrations over ζ and ξ would produce Dirac δ functions that would replace the contractions of α with Γ via D by q and p. It would represent an ideal homodyning measurement process whereby the Wigner functional $W[\alpha]$ is converted to the observed Wigner function $W'(q, p)$, in which the functional integration replaces a two-dimensional subset of the degrees

of freedom inside the Wigner functional by q and p and trace over all the other degrees of freedom.

The question is how to deal with the functional integration. For that, we need to consider the effect of the detector kernel in more detail.

V. DETECTOR KERNEL

In general, the functional integration over α in Eq. (33) cannot be evaluated, because D is not invertible. It represents a projection operation that restricts the functional phase space to those functions that can be detected. Even if we discard the quadratic term, the remaining part of the argument in the exponent does not represent the entire functional phase space. The projection induced by the overlap with Γ is in general even more restrictive than the projection associated with D. To evaluate the functional integration, we need to separate the integration into the subspaces defined by the projections imposed by D and Γ.

Let us denote the total functional phase space by $\mathcal{A}$, the subspace onto which D projects by $\mathcal{M}$, and the subspace associated with Γ by $\mathcal{G}$. To be more precise, we state that, for $\alpha \in \mathcal{M}$, we have $\alpha^* \diamond D \diamond \alpha \neq 0$, and, for $\alpha \in \mathcal{G}$, we have $\alpha^* \diamond \Gamma \neq 0$. In the latter two cases, there are in general still parts of α that do not satisfy the requirements.

In the absurd case when $\mathcal{G} \cap \mathcal{M} = \emptyset$, which implies that $\Gamma^* \diamond D = D \diamond \Gamma = 0$, (i.e., the detector cannot measure the mode of the local oscillator), the Γ-dependent terms in Eq. (33) are zero, leaving us with

$$W'_0(q, p) = \mathcal{N} \int W[\alpha] \exp\left[-\frac{1}{4}(\zeta^2 + \xi^2)\Delta x^2 \alpha^* \diamond D \diamond \alpha \right.$$

$$\left. + iq\xi - ip\zeta \right]\mathcal{D}^\circ[\alpha] d\zeta \, d\xi. \quad (34)$$

The result of the functional integration is a rotationally symmetric function of r, peaked at the origin—its amplitude at $r = 0$ is the trace over the entire Wigner functional of the state. The Fourier transform of this function is also a rotationally symmetric function peaked at the origin in phase space. Setting $\Delta x^2 = 0$, we get

$$W'_0(q, p) = \mathcal{N} \int W[\alpha] \exp(iq\xi - ip\zeta)\mathcal{D}^\circ[\alpha] d\zeta \, d\xi$$

$$= 4\pi^2 \delta(q)\delta(p). \quad (35)$$

For $\Delta x^2 \neq 0$, the result is a narrow function at the origin with a width given by Δx.

Contrary to the absurd case, we shall assume that

$$\mathcal{G} \subset \mathcal{M} \subset \mathcal{A}. \quad (36)$$

Then we can separate the phase space into three disjoint sets: $\mathcal{G}$, $\mathcal{M}_0$, and $\mathcal{A}_0$, where $\mathcal{M}_0$ is the part of $\mathcal{M}$ that excludes $\mathcal{G}$ and $\mathcal{A}_0$ is the part of $\mathcal{A}$ excluding $\mathcal{M}$. The functional integration over $\mathcal{A}_0$ gives the part of the state that is not seen by the detector. We can discard it, with the knowledge that the process is not trace preserving and the result needs to be normalized.

The functional integration over $\mathcal{M}_0$ produces the same result as the absurd case: An undesirable artifact centered at the origin. If the Wigner function of the state $W[\alpha]$ does not

overlap the origin, we can discard this part. However, many interesting states have Wigner functions sitting at the origin in phase space where they would be overlapped by this unwanted background term. In those cases, careful control of the modes that are detected can help to remove this unwanted term [4].

For the functional integration over $\mathcal{G}$, the integration is separated into an integration over the amplitude of Γ and a functional integration over a field variable that is orthogonal to Γ. This separation is formally introduced with the aid of an *inhomogeneous beam splitter*. The transformation imposed by such an inhomogeneous beam splitter is represented by the substitutions

$$\alpha \to P \diamond \alpha - iQ \diamond \beta, \quad \beta \to P \diamond \beta - iQ \diamond \alpha, \quad (37)$$

where $P(\mathbf{k}_1, \mathbf{k}_2) = \Gamma(\mathbf{k}_1)\Gamma^*(\mathbf{k}_2)$ and $Q = \mathbf{1} - P$ are projection kernels. The transformation is performed on the Wigner functional of the state $W[\alpha]$ multiplied by that of a vacuum state given by

$$W_{\text{vac}}[\beta] = \mathcal{N}_0 \exp(-2\|\beta\|^2). \quad (38)$$

When we apply Eq. (37) to Eq. (33) after multiplying it by Eq. (38), we obtain

$$W'_{\mathcal{G}}(q, p) = \mathcal{N} \int W'[\alpha, \beta] \exp\left[-\frac{1}{4}(\zeta^2 + \xi^2)\Delta x^2 \alpha^* \diamond P \diamond D \diamond P \diamond \alpha - \frac{1}{4}(\zeta^2 + \xi^2)\Delta x^2 \beta^* \diamond Q \diamond D \diamond Q \diamond \beta \right.$$
$$\left. + \frac{1}{\sqrt{2}}(\zeta - i\xi)\Gamma^* \diamond D \diamond P \diamond \alpha - \frac{1}{\sqrt{2}}(\zeta + i\xi)\alpha^* \diamond P \diamond D \diamond \Gamma + iq\xi - ip\zeta \right] \mathcal{D}^\circ[\alpha, \beta] d\zeta d\xi, \quad (39)$$

where

$$W'[\alpha, \beta] = W[P \diamond \alpha - iQ \diamond \beta] W_{\text{vac}}[P \diamond \beta - iQ \diamond \alpha], \quad (40)$$

and we assumed that $\Gamma^* \diamond D \diamond Q = Q \diamond D \diamond \Gamma = 0$.

The functional integral over α only involves a nontrivial state when the field variable is proportional to Γ. For the rest of the space, it is a vacuum state. The nontrivial part represents an ordinary integral over the complex-valued amplitude of the field variable that is proportional to Γ. Hence, $P \diamond \alpha(\mathbf{k}) \to \alpha_0 \Gamma(\mathbf{k})$, where α_0 is a complex variable (not a *field* variable). The remaining part of the functional integration over $\alpha(\mathbf{k})$

produces a constant that is absorbed into the normalization constant $\mathcal{N}$.

The functional integral over β can be separated in the same way. In this case, the state associated with the part of the field variable that is proportional to Γ is a vacuum state. However, in this case, we retain the full space of the functional integral because we need to maintain the invertibility of kernels that may appear in the Wigner functionals of the states.

When we apply these considerations, the expression in Eq. (39) becomes

$$W'_{\mathcal{G}}(q, p) = \mathcal{N} \int W[\beta](q_0, p_0) \exp\left[-\frac{1}{8}\Delta x^2 \eta(\zeta^2 + \xi^2)(q_0^2 + p_0^2) - \frac{1}{4}\Delta x^2(\zeta^2 + \xi^2)\beta^* \diamond D_{qq} \diamond \beta \right.$$
$$\left. + iq\xi - ip\zeta + ip_0\zeta\eta - iq_0\xi\eta \right] \mathcal{D}^\circ[\beta] dq_0 dp_0 d\zeta d\xi, \quad (41)$$

where $\eta = \Gamma^* \diamond D \diamond \Gamma$ is the quantum efficiency of the detector, $D_{qq} = Q \diamond D \diamond Q$, and we replaced the complex integration variable α_0 with

$$\alpha_0 \to \frac{1}{\sqrt{2}}(q_0 + ip_0). \quad (42)$$

The functional integration therefore splits into a reduced functional integration that runs over the subspace $\mathcal{M}$ (i.e., those field variables that can pass through D) and an integration over the complex plane.

If we discard the Δx^2 terms in Eq. (41), we would get

$$W'_{\mathcal{G}}(q, p) = \mathcal{N} \int W[\beta](q_0, p_0) \exp\left[i(q - q_0\eta)\xi \right.$$
$$\left. - i(p - p_0\eta)\zeta \right] \mathcal{D}^\circ[\beta] dq_0 dp_0 d\zeta d\xi$$
$$= \mathcal{N} \int W[\beta]\left(\frac{q}{\eta}, \frac{p}{\eta} \right) \mathcal{D}^\circ[\beta]. \quad (43)$$

The final functional integration over β traces out all those degrees of freedom that are not associated with Γ. The result

shows the effect of the detection efficiency η. It produces a scaling of the Wigner functional, which can be removed through a redefinition of the variables, provided that η is known.

The separation of the different subspaces is governed by the nature of the detectors. There are different special cases that we can consider. Here, we consider the two extreme cases mentioned in the Appendix: A bucket detector and a single-mode detector.

A. Bucket detector

If the detector is a bucket detector, then we can set $D(\mathbf{k}_1, \mathbf{k}_2) = \eta \mathbf{1}(\mathbf{k}_1, \mathbf{k}_2)$, where η is the quantum efficiency of the detector, and $\mathbf{1}(\mathbf{k}_1, \mathbf{k}_2)$ is the identity. In terms of the subspaces, we then have $\mathcal{M}_0 \cong \mathcal{A}_0$, because all the elements in the functional phase space can be detected by the bucket detector. As a result, there are only two subspaces: $\mathcal{G}$ and $\mathcal{M}_0 \cong \mathcal{A}_0$.

The effect on the expressions in Eq. (34) and Eq. (41) is that $\alpha^* \diamond D \diamond \alpha \rightarrow \eta \|\alpha\|^2$ and $D_{qq} \rightarrow \eta Q$, respectively. For further simplifications, we need to specify the initial Wigner functional. The coherent state is considered below as an example for this case.

B. Single-mode detector

Alternatively, we consider D as a single-mode detector kernel $D(\mathbf{k}_1, \mathbf{k}_2) = \eta M(\mathbf{k}_1)M^*(\mathbf{k}_2)$, where $M(\mathbf{k})$ is the normalized angular spectrum of the detector's mode and η is again the quantum efficiency of the detector. In this case, we assume that $M(\mathbf{k}) = \Gamma(\mathbf{k})$. There are again only two subspaces: $\mathcal{A}_0$ and $\mathcal{G} \cong \mathcal{M}$. In this case, there is no equivalent for the absurd case in Eq. (34). The single-mode detector is preferred when the Wigner functional of the state overlaps the origin in phase space.

Since $\beta^* \diamond D_{qq} \diamond \beta = \beta^* \diamond Q \diamond \Gamma\Gamma^* \diamond Q \diamond \beta = 0$, the integration over the subspace $\mathcal{G}$, with a subsequent normalization, produces

$$
\begin{aligned}
W'_{\mathcal{G}}(q, p) = \frac{1}{(2\pi)^2} \int W_0(q_0, p_0) \exp\bigg[& iq\xi - ip\zeta \\
& - \frac{1}{8}\Delta x^2 \eta(\zeta^2 + \xi^2)(q_0^2 + p_0^2) \\
& + ip_0\zeta\eta - iq_0\xi\eta \bigg] dq_0 dp_0 d\zeta d\xi,
\end{aligned}
\tag{44}
$$

where we traced over β and defined

$$
\int W[\beta](q_0, p_0)\mathcal{D}^\circ[\beta] = W_0(q_0, p_0).
\tag{45}
$$

The integrations over ζ and ξ evaluate to

$$
\begin{aligned}
W'_{\mathcal{G}}(q, p) = \int \exp\bigg[& -2\frac{(q_0\eta - q)^2 + (p_0\eta - p)^2}{(q_0^2 + p_0^2)\Delta x^2 \eta} \bigg] \\
& \times \frac{2W_0(q_0, p_0)}{(q_0^2 + p_0^2)\pi \Delta x^2 \eta} \, dq_0 dp_0.
\end{aligned}
\tag{46}
$$

The observed Wigner function is thus obtained from the traced Wigner functional through a linear integral operation (superposition integral) with a kernel given by

$$
\begin{aligned}
\kappa(q_0, p_0, q, p) = \exp\bigg[& -2\frac{(q_0\eta - q)^2 + (p_0\eta - p)^2}{(q_0^2 + p_0^2)\Delta x^2 \eta} \bigg] \\
& \times \frac{2}{(q_0^2 + p_0^2)\pi \Delta x^2 \eta}.
\end{aligned}
\tag{47}
$$

There is also a scaling introduced by the quantum efficiency η, as in Eq. (43). This scaling can be removed from Eq. (46) through the redefinitions $\{q, p\} \rightarrow \{q'\eta, p'\eta\}$, and a renormalization, leading to

$$
\begin{aligned}
W'_{\mathcal{G}}(q', p') = \int \exp\bigg[& -2\eta \frac{(q_0 - q')^2 + (p_0 - p')^2}{(q_0^2 + p_0^2)\Delta x^2} \bigg] \\
& \times \frac{2\eta W_0(q_0, p_0)}{(q_0^2 + p_0^2)\pi \Delta x^2} \, dq_0 dp_0.
\end{aligned}
\tag{48}
$$

The quantum efficiency is now associated with Δx and represents a slight reduction in the effective number of photons in the local oscillator.

Without the factors of $q_0^2 + p_0^2$ in the denominators, Eq. (47) would represent a Dirac δ function in the limit $\Delta x \rightarrow 0$. However, the factors of $q_0^2 + p_0^2$ in the denominators make the kernel dependent on the distance from the origin. When $\{q, p\} = 0$, the kernel is singular at the origin as a function of $\{q_0, p_0\}$. For fixed values of $\{q, p\} \neq 0$, and a small value for Δx, the kernel gives a narrow Gaussian peak located at $\{q_0, p_0\} = \{q\eta^{-1}, p\eta^{-1}\}$. It becomes broader as the point $\{q, p\}$ moves further away from the origin. In fact, the kernel has a scale invariance: we can multiply all the variables by the same factor and it will cancel apart from an overall change in the amplitude of the kernel. It implies that the width of the peak scales linearly with the distance of the peak from the origin. The peak would thus become comparable to the minimum uncertainty area when $q_0^2 + p_0^2 \sim \zeta_0^2$—i.e., when the average number of photons in the state becomes comparable to the average number of photons in the local oscillator.

Due to the factor of $q_0^2 + p_0^2$ in the denominators, the integrals in Eq. (46) tend to be intractable. If Δx is small enough, we can argue that for $\{q, p\} > 0$, the kernel becomes zero whenever $\{q_0, p_0\}$ differs by more than Δx from the location of its peak. Therefore, we can substitute $q_0^2 + p_0^2 \rightarrow (q^2 + p^2)\eta^{-2}$, which makes the integration over $\{q_0, p_0\}$ more tractable. The expression in Eq. (46) then becomes

$$
\begin{aligned}
W'_{\mathcal{G}}(q, p) \approx \int \exp\bigg[& -2\eta \frac{(q_0\eta - q)^2 + (p_0\eta - p)^2}{(q^2 + p^2)\Delta x^2} \bigg] \\
& \times \frac{2\eta W_0(q_0, p_0)}{(q^2 + p^2)\pi \Delta x^2} \, dq_0 dp_0,
\end{aligned}
\tag{49}
$$

which is now similar to a convolution, where the resolution of the observed Wigner function is determined by the ratio of the average number of photons in the state to the average number of photons in the local oscillator after the reduction imposed by the detection efficiency.

VI. EXAMPLE: COHERENT STATE

As a first example, we consider the homodyne tomography of an arbitrary coherent state. The transformation of the inhomogeneous beam splitter is performed on the Wigner functional of the coherent state (1) times that of a vacuum state (38) by substituting Eq. (37) into the combined Wigner functional of the state and the vacuum. The effect is

$$
\begin{aligned}
\mathcal{N}_0^2 \exp(-2\|\alpha - \varphi\|^2 & - 2\|\beta\|^2) \\
& \rightarrow \mathcal{N}_0 \exp(-2\|\alpha - P \diamond \varphi\|^2) \\
& \times \mathcal{N}_0 \exp(-2\|\beta - Q \diamond \varphi\|^2),
\end{aligned}
\tag{50}
$$

where $\varphi(\mathbf{k})$ is the spectral parameter function of the coherent state. After we trace out the degrees of freedom of α that are orthogonal to Γ, the result reads

$$
\begin{aligned}
W_c[\beta](\alpha_0) = {} & 2\exp(-2|\alpha_0 - \alpha_1|^2) \\
& \times \mathcal{N}_0 \exp(-2\|\beta - \beta_1\|^2),
\end{aligned}
\tag{51}
$$

where $\alpha_1 = \Gamma^* \diamond \varphi$ is the complex coefficient for the part of φ proportional to Γ, and $\beta_1 = Q \diamond \varphi$ is a complex function representing the part of φ that is orthogonal to Γ. After substituting Eq. (51) into Eq. (41), we obtain

$$
W_c(q, p) = \frac{\mathcal{N}_0}{2\pi^2} \int \exp\left[-(q_0 - q_1)^2 - (p_0 - p_1)^2\right.
$$
$$
- \frac{1}{8}\Delta x^2 \eta(\zeta^2 + \xi^2)(q_0^2 + p_0^2) + ip_0\zeta\eta - iq_0\xi\eta
$$
$$
+ iq\xi - ip\zeta - \frac{1}{4}\Delta x^2(\zeta^2 + \xi^2)\beta^* \diamond D_{qq} \diamond \beta
$$
$$
\left. - 2\|\beta - \beta_1\|^2\right]\mathcal{D}^\circ[\beta]dq_0 dp_0 d\zeta d\xi, \tag{52}
$$

where we expressed α_0 in terms of q_0 and p_0, and replaced $\alpha_1 \to \frac{1}{\sqrt{2}}(q_1 + ip_1)$. The integrations over q_0 and p_0 are separated from the functional integration over β.

A. Bucket detector

For the bucket detector, we replace $D_{qq} \to \eta Q$ in Eq. (52) and evaluate the functional integration over β and the integrations over q_0 and p_0. The result is

$$
W'_\mathcal{G}(q, p) = \int \exp\left[-\frac{1}{4}\frac{(\xi\eta + i2q_1)^2 + (\zeta\eta - i2p_1)^2}{1 + \tau}\right.
$$
$$
\left. - q_1^2 - p_1^2 + iq\xi - ip\zeta - 2\frac{\tau}{1 + \tau}\|\beta_1\|^2\right]
$$
$$
\times \frac{1}{2\pi(1 + \tau)^\Omega} d\zeta d\xi, \tag{53}
$$

where $\Omega = \mathrm{tr}\{Q\} + 1$, and

$$
\tau = \frac{1}{8}(\zeta^2 + \xi^2)\eta\Delta x^2. \tag{54}
$$

Since τ contains the radial dependence of the remaining integration variables, the factor of $1/(1 + \tau)^\Omega$ restricts the integration domain that would contribute to a region close to the origin. Therefore, we can set $1 + \tau \to 1$ and evaluate the remaining integration. Hence,

$$
W'_\mathcal{G}(q, p) \approx \frac{1}{2\pi} \int \exp\left[-\frac{1}{4}(\xi\eta + i2q_1)^2 - \frac{1}{4}(\zeta\eta - i2p_1)^2\right.
$$
$$
- q_1^2 - p_1^2 + iq\xi - ip\zeta
$$
$$
\left. - \frac{1}{4}(\zeta^2 + \xi^2)\eta\Delta x^2\|\beta_1\|^2\right]d\zeta d\xi
$$
$$
= \frac{2}{\eta^2 + \eta\Delta x^2\|\beta_1\|^2}
$$
$$
\times \exp\left(-2\frac{|\alpha - \eta\alpha_1|^2}{\eta^2 + \eta\Delta x^2\|\beta_1\|^2}\right), \tag{55}
$$

where we expressed the result in terms of αs at the end. If we set $\Delta x = 0$, the result is a scaled version of the original coherent state. As before, we compensate for the scaling by redefining the variable $\alpha \to \alpha'\eta$ and renormalizing the function. The result becomes

$$
W'_\mathcal{G}(\alpha') = \frac{2}{1 + \Delta w} \exp\left(\frac{-2|\alpha' - \alpha_1|^2}{1 + \Delta w}\right), \tag{56}
$$

where

$$
\Delta w = \frac{\Delta x^2\|\beta_1\|^2}{\eta} = \frac{\|Q \diamond \varphi\|^2}{\eta\zeta_0^2}. \tag{57}
$$

We see that the width of the rescaled state is increased by the ratio of the number of photons that can pass through Q over the number of photons in the local oscillator, reduced by the quantum efficiency.

B. Single-mode detector

For a single-mode detector with $M(\mathbf{k}) = \Gamma(\mathbf{k})$, we get $\beta^* \diamond D_{qq} \diamond \beta = |\Gamma^* \diamond Q \diamond \beta|^2 = 0$. The functional integration over β can be evaluated without complications. So, Eq. (52) becomes

$$
W_{\mathrm{coh}}(q, p) = \frac{1}{2\pi^2} \int \exp\left[-(q_0 - q_1)^2 - (p_0 - p_1)^2\right.
$$
$$
- \frac{1}{8}\Delta x^2 \eta(\zeta^2 + \xi^2)(q_0^2 + p_0^2) + iq\xi - ip\zeta
$$
$$
\left. + ip_0\zeta\eta - iq_0\xi\eta\right]dq_0 dp_0 d\zeta d\xi. \tag{58}
$$

If we first evaluate the integration over q_0 and p_0, as in the bucket detector case, we again get factors of $1 + \tau$ in the denominator but this time the dependence is not as severely suppressed, which implies that the approximation $1 + \tau \approx 1$ is not as valid. Therefore, we first integrate over ζ and ξ to obtain

$$
W'_\mathcal{G}(q, p) = \int 4 \exp\left[-(q_0 - q_1)^2 - (p_0 - p_1)^2\right]
$$
$$
\times \exp\left[-2\frac{(q_0\eta - q)^2 + (p_0\eta - p)^2}{(q_0^2 + p_0^2)\eta\Delta x^2}\right]
$$
$$
\times \frac{1}{(q_0^2 + p_0^2)\pi\eta\Delta x^2} dq_0 dp_0, \tag{59}
$$

which corresponds to Eq. (46). It can be assumed that the kernel peak is narrow enough for small Δx so that we can substitute $q_0^2 + p_0^2 \to (q^2 + p^2)\eta^{-2}$, as before. The integrals over q_0 and p_0 can then be evaluated to give

$$
W'_\mathcal{G}(q, p) = \frac{2\eta}{\eta^3 + |\alpha|^2\Delta x^2} \exp\left(-2\frac{\eta|\alpha - \eta\alpha_1|^2}{\eta^3 + |\alpha|^2\Delta x^2}\right), \tag{60}
$$

where we converted the expression back to complex-valued variables. We recover a scaled version of the Wigner function for the coherent states, but with a different width. If we set $\Delta x = 0$, the result is a scaled version of the original coherent state due to the reduced efficiency represented by η. Compensating for the scaling by redefining the complex variable $\alpha \to \alpha'\eta$, we obtain

$$
W'_\mathcal{G}(\alpha') = \frac{2}{1 + \frac{1}{\eta}|\alpha'|^2\Delta x^2} \exp\left(-2\frac{|\alpha' - \alpha_1|^2}{1 + \frac{1}{\eta}|\alpha'|^2\Delta x^2}\right). \tag{61}
$$

For large enough $|\alpha_1|$, we can replace $|\alpha'|^2 \to |\alpha_1|^2$ in the denominators. The result then has the same form as in Eq. (56), but this time the increase in width is given by the ratio of the average number of photons in the state that can be observed

by the detector to the reduced average number of photons in the local oscillator:

$$\Delta w = \frac{\Delta x^2 |\alpha_1|^2}{\eta} = \frac{|\Gamma^* \diamond \varphi|^2}{\eta \zeta_0^2}. \tag{62}$$

VII. EXAMPLE: FOCK STATES

Since the Wigner functionals of Fock states are centered at the origin of phase space, we only consider the single-mode detector. The generating function for the Wigner functionals of the single-mode Fock states is derived in the Appendix and given in Eq. (A8). After combining it with the Wigner functional for the vacuum state in Eq. (38), and applying Eq. (37) to separate the integration domains, we obtain

$$\mathcal{W}[\alpha, \beta](J) = \frac{\mathcal{N}_0^2}{1+J} \exp \left[i2\mathcal{H}\beta^* \diamond Q \diamond FF^* \diamond P \diamond \alpha \right.$$
$$- i2\mathcal{H}\alpha^* \diamond P \diamond FF^* \diamond Q \diamond \beta$$
$$- 2\alpha^* \diamond (\mathbf{1} - \mathcal{H}P \diamond FF^* \diamond P) \diamond \alpha$$
$$\left. - 2\beta^* \diamond (\mathbf{1} - \mathcal{H}Q \diamond FF^* \diamond Q) \diamond \beta \right], \tag{63}$$

where

$$\mathcal{H} = \frac{2J}{1+J}. \tag{64}$$

Here, we are interested in the case when the parameter function of the Fock states does not exactly match the mode of the local oscillator. Therefore, we assume that $F(\mathbf{k}) = \mu\Gamma(\mathbf{k}) + \nu\Lambda(\mathbf{k})$, where $|\mu|^2 + |\nu|^2 = 1$, $\Gamma^* \diamond \Lambda = P \diamond \Lambda = 0$, and $Q \diamond \Lambda = \Lambda$. As a result, $|\mu|^2$ is the overlap efficiency. After integrating out the part of the α-dependent functional orthogonal to Γ, we obtain

$$\mathcal{W}[\beta](\alpha_0, J) = \frac{2\mathcal{N}_0}{1+J} \exp[-2(1 - \mathcal{H}|\mu|^2)|\alpha_0|^2$$
$$+ i2\mathcal{H}\mu^*\nu\alpha_0\beta^* \diamond \Lambda - i2\mathcal{H}\mu\nu^*\alpha_0^*\Lambda^* \diamond \beta$$
$$- 2\beta^* \diamond \mathcal{K} \diamond \beta]. \tag{65}$$

where

$$\mathcal{K} = \mathbf{1} - \mathcal{H}|\nu|^2 \Lambda\Lambda^*. \tag{66}$$

The functional integration over β implies tracing the state over β, which produces

$$\mathcal{W}(\alpha_0, J) = \frac{2}{(1+J)\det\{\mathcal{K}\}} \exp[-2(1 - \mathcal{H}|\mu|^2)|\alpha_0|^2$$
$$+ 2\mathcal{H}^2 |\mu|^2 |\nu|^2 |\alpha_0|^2 \Lambda^* \diamond \mathcal{K}^{-1} \diamond \Lambda]. \tag{67}$$

The determinant and inverse can be simplified as

$$\det\{\mathcal{K}\} = \det\{\mathbf{1} - \mathcal{H}|\nu|^2 \Lambda\Lambda^*\} = 1 - \mathcal{H}|\nu|^2,$$
$$\mathcal{K}^{-1} = (\mathbf{1} - \mathcal{H}|\nu|^2 \Lambda\Lambda^*)^{-1} = \mathbf{1} + \frac{\mathcal{H}|\nu|^2 \Lambda\Lambda^*}{1 - \mathcal{H}|\nu|^2}. \tag{68}$$

Therefore, the expression becomes

$$\mathcal{W}(\alpha_0, J) = \frac{2 \exp(-2|\alpha_0|^2)}{1+J\omega} \exp\left(\frac{4J|\mu|^2|\alpha_0|^2}{1+J\omega}\right), \tag{69}$$

where we used $|\nu|^2 = 1 - |\mu|^2$ to define

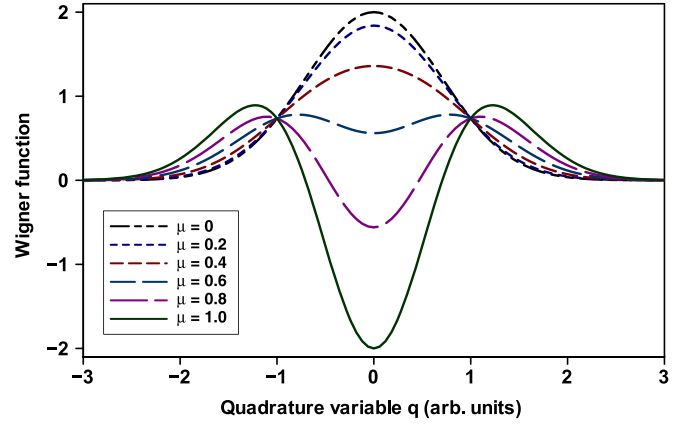$$\omega = 1 - 2|\nu|^2 = 2|\mu|^2 - 1 = |\mu|^2 - |\nu|^2. \tag{70}$$

FIG. 2. Observed Wigner function of a single-photon Fock state as a function q with $p = 0$ for different values of $|\mu|$.

We replace $W_0(q_0, p_0)$ in Eq. (49) by the generating function in Eq. (69) to compute a generating function for the observed Wigner functions of the Fock states:

$$\mathcal{W}_F(\alpha, J) = \int \exp\left[-\frac{1 + J\omega - 2J|\mu|^2}{1 + J\omega}(q_0^2 + p_0^2)\right]$$
$$\times \exp\left[-2\eta \frac{(q_0\eta - q)^2 + (p_0\eta - p)^2}{(q^2 + p^2)\Delta x^2}\right]$$
$$\times \frac{4\eta}{(1 + J\omega)(q^2 + p^2)\pi \Delta x^2} dq_0 dp_0$$
$$= \exp\left[-\frac{2(1 - J)|\alpha|^2\eta}{(1 - J)|\alpha|^2 \Delta x^2 + (1 + J\omega)\eta^3}\right]$$
$$\times \frac{2\eta}{(1 - J)|\alpha|^2 \Delta x^2 + (1 + J\omega)\eta^3}. \tag{71}$$

The expression already incorporates the approximation where we set $q_0^2 + p_0^2 \rightarrow (q^2 + p^2)\eta^{-2}$ in the denominator.

Since the Wigner functions of the Fock states are located at the origin, we can assume that $|\alpha|^2 \Delta x^2 \ll 1$. Therefore, we can set $\Delta x^2 = 0$. The expression then simplifies to

$$\mathcal{W}(\alpha, J) = \frac{2}{(1 + J\omega)\eta^2} \exp\left[-\frac{2|\alpha|^2}{\eta^2} + \frac{4J|\mu|^2|\alpha|^2}{(1 + J\omega)\eta^2}\right]. \tag{72}$$

When we redefine $\alpha \rightarrow \alpha'\eta$ to remove that scaling caused by η, we recover Eq. (69). The Wigner functions of the individual Fock states are then given by

$$W_{|n\rangle\langle n|}(\alpha') = (1 - 2|\mu|^2)^n \exp(-2|\alpha'|^2)L_n\left(\frac{4|\mu|^2|\alpha'|^2}{2|\mu|^2 - 1}\right), \tag{73}$$

where $L_n(\cdot)$ is the nth order Laguerre polynomial. For $|\mu| < 1$, it is scaled relative to the Gaussian envelope. In Fig. 2, we show the observed Wigner function of a single-photon Fock state for different values of $|\mu|$, ranging from that of the Fock state (for $|\mu| = 1$) to that of a vacuum state (for $|\mu| = 0$). The curves in Fig. 2, correspond to those in Fig. 3(b) of Ref. [4], but with the role of η being replaced by $|\mu|$ in our case.

Marginal distributions

We can use the generating function in Eq. (69) to investigate the marginal distributions of the Wigner function that it produces. The variable α is expressed in terms of q and p, and the resulting expression is integrated over p to produce a generating function for the observed marginal distributions as a function of q. It is given by

$$
\mathcal{W}(q, J) = \int \mathcal{W}(q, p, J) \frac{dp}{2\pi}
$$
$$
= \frac{1}{\sqrt{\pi(1-J)(1+J\omega)}} \exp\left(-q^2 + \frac{2J|\mu|^2 q^2}{1+J\omega}\right).
$$
(74)

The observed marginal distribution for the single-photon Fock state is

$$
\partial_J \mathcal{W}(q, J)|_{J=0} = \frac{\exp(-q^2)}{\sqrt{\pi}}(2|\mu|^2 q^2 + 1 - |\mu|^2). \quad (75)
$$

It is a non-negative function for all the allowed values of $|\mu|$ (i.e., $0 \leqslant |\mu| \leqslant 1$). For $|\mu| = 1$, the distribution is zero at the origin, but for smaller values of $|\mu|$ it is larger than zero at the origin.

We can compare this result with what would be obtained from a naive approach where we simply substitute $\alpha(\mathbf{k}) \to \alpha\Gamma(\mathbf{k})$ into the generating function for Wigner functionals of the Fock states (A8) to get

$$
\mathcal{W}'(\alpha, J) = \frac{2}{1+J} \exp\left(-2|\alpha|^2 + \frac{4J|\mu|^2}{1+J}|\alpha|^2\right) \quad (76)
$$

instead of Eq. (69). After applying the same integration over p to produce the generating function for the marginal distributions, we obtain

$$
\mathcal{W}'(q, J) = \frac{1}{\sqrt{\pi(1+J)(1-J\omega)}} \exp\left(-q^2 + \frac{2J|\mu|^2 q^2}{1+J}\right).
$$
(77)

In this case, the marginal distribution for the single-photon Fock state is

$$
\partial_J \mathcal{W}'(q, J)|_{J=0} = \frac{\exp(-q^2)}{\sqrt{\pi}}(2|\mu|^2 q^2 - 1 + |\mu|^2). \quad (78)
$$

At the origin, this function is negative for $|\mu|^2 < 1$, which represents a nonphysical situation. Therefore, the naive approach does not in general give valid Wigner functions.

VIII. EXAMPLE: SQUEEZED VACUUM STATE

As a final example, we consider the homodyne tomography process of a squeezed vacuum state, using single-mode detection. A pure squeezed vacuum state has a Wigner functional given by

$$
W_{\mathrm{sv}}[\alpha] = \mathcal{N}_0 \exp(-2\alpha^* \diamond A \diamond \alpha
$$
$$
- \alpha^* \diamond B \diamond \alpha^* - \alpha \diamond B^* \diamond \alpha), \quad (79)
$$

where A and B are kernel functions depending on a squeezing parameter Ξ.

If we naively express the observed Wigner function as that which is obtained by substituting $\alpha(\mathbf{k}) \to \alpha_0 \Gamma(\mathbf{k})$ into

Eq. (79), it would read

$$
W_{\mathrm{nsv}}(\alpha_0) = \mathcal{N} \exp\left(-2|\alpha_0|^2 g_A - \alpha_0^{*2} g_B - \alpha_0^2 g_B^*\right), \quad (80)
$$

where $\mathcal{N}$ is a normalization constant, and

$$
g_A = \Gamma^* \diamond A \diamond \Gamma, \quad g_B = \Gamma^* \diamond B \diamond \Gamma^*, \quad g_B^* = \Gamma \diamond B^* \diamond \Gamma.
$$
(81)

However, the trace over β can introduce distortions to this function, as shown below.

We first perform the separation of the functional phase space by using the transformation given in Eq. (37). Then, we integrate out the part of the state that depends on α and is orthogonal to Γ. The result is

$$
W_{\mathrm{sv}}[\beta](\alpha_0) = 2 \exp\left(-2|\alpha_0|^2 g_A - \alpha_0^{*2} g_B - \alpha_0^2 g_B^*\right)
$$
$$
\times \mathcal{N}_0 \exp[-2\beta^* \diamond A_q \diamond \beta + \beta^* \diamond B_{qq} \diamond \beta^*
$$
$$
+ \beta \diamond B_{qq}^* \diamond \beta - i2\beta^* \diamond (U\alpha_0 + V\alpha_0^*)
$$
$$
+ i2(\alpha_0^* U^* + \alpha_0 V^*) \diamond \beta], \quad (82)
$$

where

$$
E_{qq} = Q \diamond E \diamond Q, \quad B_{qq} = Q \diamond B \diamond Q^*,
$$
$$
B_{qq}^* = Q^* \diamond B^* \diamond Q, \quad A_q = \mathbf{1} + E_{qq}, \quad (83)
$$

with $E = A - \mathbf{1}$, and

$$
U = Q \diamond E \diamond \Gamma, \quad V = Q \diamond B \diamond \Gamma^*, \quad (84)
$$

are functions orthogonal to Γ. They are included because Γ is generally not an eigenfunction of the kernels. The kernels transform Γ as follows:

$$
E \diamond \Gamma = P \diamond E \diamond \Gamma + Q \diamond E \diamond \Gamma = g_E \Gamma + U,
$$
$$
B \diamond \Gamma^* = P \diamond B \diamond \Gamma^* + Q \diamond B \diamond \Gamma^* = g_B \Gamma + V, \quad (85)
$$

where $g_E = \Gamma^* \diamond E \diamond \Gamma = g_A - 1$.

The first line in Eq. (82) contains the result that we obtained from the naive approach, given in Eq. (80). Hence, we can represent Eq. (82) as

$$
W_{\mathrm{sv}}[\beta](\alpha_0) = W_{\mathrm{nsv}}(\alpha_0) W_\beta[\beta](\alpha_0). \quad (86)
$$

Since the β-dependent part also contains α_0, the trace over β generally produces an α_0-dependent function that modifies $W_{\mathrm{nsv}}(\alpha_0)$ and thereby distorts it.

The single-mode detector with $M(\mathbf{k}) = \Gamma(\mathbf{k})$ leads to $\beta^* \diamond D_{qq} \diamond \beta = 0$. Therefore, the functional integral over β implies the trace of the state over β. Considering only the β-dependent part of the expression, we obtain

$$
W_\beta'(\alpha_0) = \int W_\beta[\beta](\alpha_0) \mathcal{D}^\circ[\beta]
$$
$$
= (\det\{A_q\} \det\{K\})^{-1/2} \exp\left[\psi^* \diamond A_q^{-1} \diamond \psi\right.
$$
$$
+ \left(\psi - \psi^* \diamond A_q^{-1} \diamond B_{qq}\right) \diamond K^{-1}
$$
$$
\times \diamond\left(\psi^* - B_{qq}^* \diamond A_q^{-1} \diamond \psi\right)], \quad (87)
$$

where

$$
\psi = U\alpha_0 + V\alpha_0^*, \quad K = A_q^* - B_{qq}^* \diamond A_q^{-1} \diamond B_{qq}. \quad (88)
$$

The result in Eq. (87) can be represented as

$$
W_\beta'(\alpha_0) = \mathcal{N}_\beta \exp\left(2|\alpha_0|^2 h_A + \alpha_0^{*2} h_B + \alpha_0^2 h_B^*\right), \quad (89)
$$

where

$$\mathcal{N}_\beta = (\det\{A_q\} \det\{K\})^{-1/2},$$

$$h_A = U^* \diamond A_q^{-1} \diamond U + V^* \diamond A_q^{-1} \diamond V$$
$$+ \Psi_u^* \diamond K^{-1} \diamond \Psi_u + \Psi_v^* \diamond K^{-1} \diamond \Psi_v,$$

$$h_B = U^* \diamond A_q^{-1} \diamond V + \Psi_u^* \diamond K^{-1} \diamond \Psi_v,$$

$$h_B^* = V^* \diamond A_q^{-1} \diamond U + \Psi_v^* \diamond K^{-1} \diamond \Psi_u, \tag{90}$$

with

$$\Psi_u = B_{qq}^* \diamond A_q^{-1} \diamond U - V^*, \quad \Psi_v = B_{qq}^* \diamond A_q^{-1} \diamond V - U^*. \tag{91}$$

The combination of Eq. (89) with the β-independent part of Eq. (82) becomes

$$W'_{\text{sv}}(\alpha_0) = 2\mathcal{N}_\beta \exp\big[-2|\alpha_0|^2(g_A - h_A)$$
$$- \alpha_0^{*2}(g_B - h_B) - \alpha_0^2(g_B^* - h_B^*)\big]. \tag{92}$$

The observed Wigner function is determined by substituting Eq. (92) in the place of $W_0(q_0, p_0)$ in Eq. (49), which assumes a small Δx^2. Here, we set $\eta = 1$, because the effect of η is the same as in the previous cases. After evaluating the integrals, we obtain

$$W_{\text{osv}}(\alpha) = \frac{2\mathcal{N}_\beta}{\sqrt{g_D}} \exp\bigg(-2|\alpha|^2 g_C - 2|\alpha|^2 \frac{g_A - h_A - g_C}{g_D}$$
$$- \alpha^{*2} \frac{g_B - h_B}{g_D} - \alpha^2 \frac{g_B^* - h_B^*}{g_D}\bigg), \tag{93}$$

where we discarded the Δx^4 terms and defined

$$g_C = \frac{(g_A - h_A)^2 - |g_B - h_B|^2}{2(g_A - h_A)},$$

$$g_D = 1 + 2|\alpha|^2 (g_A - h_A)\Delta x^2. \tag{94}$$

If we set $\Delta x = 0$, the expression becomes the same as in Eq. (92). Therefore, the distortions cannot be removed by increasing the power in the local oscillator.

A. Weakly squeezed vacuum state

The complexity of the expression in Eq. (92), as represented by the quantities in Eq. (90), indicates that the observed Wigner function of a squeezed vacuum state could in general be severely distorted. However, it may be reasonable to expect that the distortions would be reduced if the state is only weakly squeezed. To investigate this possibility, we consider a squeezing parameter Ξ that is small. Then we can expand the kernels and keep only terms up to second order in Ξ. As a result, $A \approx \mathbf{1} + E_2$ and $A^{-1} \approx \mathbf{1} - E_2$, where E_2 is second order in Ξ, and B and B^* are first order in Ξ. We also define $U = g_U U_0$ and $V = g_V V_0$, so that

$$E_2 \diamond \Gamma = g_E \Gamma + g_U U_0, \quad B \diamond \Gamma^* = g_B \Gamma + g_V V_0, \tag{95}$$

where U_0 and V_0 are normalized functions.

By replacing $Q \to \mathbf{1} + \Gamma\Gamma^*$ and using Eqs. (83) and (85), we have

$$A_q = \mathbf{1} + E_2 - g_E \Gamma\Gamma^* - g_U U_0 \Gamma^* - g_U^* \Gamma U_0^*,$$

$$A_q^{-1} \approx \mathbf{1} - E_2 + g_E \Gamma\Gamma^* + g_U U_0 \Gamma^* + g_U^* \Gamma U_0^*. \tag{96}$$

The purity of the initial squeezed vacuum states implies that, to second order in Ξ,

$$B \diamond B^* \approx 2E_2. \tag{97}$$

Therefore, the expressions for K and its inverse become

$$K \approx \mathbf{1} - E_2 + g_E \Gamma^*\Gamma + g_U \Gamma^* U_0 + g_U^* U_0^* \Gamma + |g_V|^2 V_0^* V_0,$$

$$K^{-1} \approx \mathbf{1} + E_2 - g_E \Gamma^*\Gamma - g_U \Gamma^* U_0 - g_U^* U_0^* \Gamma - |g_V|^2 V_0^* V_0. \tag{98}$$

To second order in Ξ, the product of determinants is

$$\det\{A_q\}\det\{K\} = \det\{A_q \diamond K\}$$
$$\approx \det\{\mathbf{1} + |g_V|^2 V_0 V_0^*\}$$
$$= 1 + |g_V|^2. \tag{99}$$

Here, it is assumed that $|g_V| < 1$, otherwise the expansion would not be convergent. Although the identity $\mathbf{1}$ is infinite dimensional, by itself it just gives $\mathbf{1}^\Omega = 1$. The only part that deviates from $\mathbf{1}$ is one dimensional. Therefore, the power becomes 1.

Since the leading contribution in ψ is first order in Ξ, the expansion of the exponent in Eq. (87) to second order in Ξ implies that the inverses become $A_q^{-1} \to \mathbf{1}$ and $K^{-1} \to \mathbf{1}$. Moreover, all the terms in Eq. (90) that contain U are dropped because they are already second order in Ξ.

The first term in the exponent in Eq. (87) becomes

$$\psi^* \diamond A_q^{-1} \diamond \psi \approx \psi^* \diamond \psi \approx |\alpha_0|^2 |g_V|^2, \tag{100}$$

to second order in Ξ. Since ψ and B_{qq} are first order in Ξ and orthogonal to Γ, it follows that

$$B_{qq}^* \diamond A_q^{-1} \diamond \psi \approx g_V B^* \diamond V_0 \alpha_0^*,$$
$$\psi^* \diamond A_q^{-1} \diamond B_{qq} \approx g_V^* V_0^* \diamond B\alpha, \tag{101}$$

which are at least second order in Ξ. Therefore, the second term in the exponent also becomes

$$(\psi - \psi^* \diamond A_q^{-1} \diamond B_{qq}) \diamond K^{-1} \diamond (\psi^* - B_{qq}^* \diamond A_q^{-1} \diamond \psi)$$
$$\approx \psi^* \diamond \psi \approx |\alpha_0|^2 |g_V|^2. \tag{102}$$

The expression in Eq. (87) thus reads

$$W'_\beta(\alpha_0) = \frac{\exp\left(2|\alpha_0|^2 |g_V|^2\right)}{1 + |g_V|}. \tag{103}$$

For a quantitative analysis of $|g_V|$, we use previously obtained results [18]. When the mode size of the local oscillator is much smaller than that of the pump beam, the bandwidth of the local oscillator is much larger than that of the pump beam, and thin-crystal conditions apply; the overlaps of the kernels by the mode of the local oscillator are given by

$$g_A = \Gamma^* \diamond A \diamond \Gamma = \cosh(\Xi) = 1 + g_E,$$

$$g_B = \Gamma^* \diamond B \diamond \Gamma^* = \sinh(\Xi), \tag{104}$$

where we discarded a phase factor associated with B. It then follows from Eq. (97) that

$$|g_V|^2 \approx 2g_E - |g_B|^2 = -[\cosh(\Xi) - 1]^2 \approx O(\Xi^4). \quad (105)$$

As a result, we can set $|g_V|^2 = 0$. The observed Wigner function for a weakly squeezed vacuum state therefore corresponds to the naive case give in Eq. (80).

B. Single-mode squeezing

In those cases where highly squeezed states have been produced, the experimental conditions usually imply that the state represents a single mode [24]. When the down-conversion efficiency (squeezing parameter) is increased by strongly focusing the pump beam into the nonlinear crystal so that the Rayleigh range of the pump beam becomes comparable to the length of the crystal, the Schmidt number of the down-converted state becomes close to 1 [25]. Under such conditions, the kernels of the squeezed state can be represented by

$$A(\mathbf{k}_1, \mathbf{k}_2) = \mathbf{1}(\mathbf{k}_1, \mathbf{k}_2) + 2\sinh^2\left(\frac{1}{2}\Xi\right)\Theta(\mathbf{k}_1)\Theta^*(\mathbf{k}_2),$$

$$B(\mathbf{k}_1, \mathbf{k}_2) = \sinh(\Xi)\Theta(\mathbf{k}_1)\Theta(\mathbf{k}_2), \quad (106)$$

where Θ is the mode of the state.

If we assume that the mode of the state is the same as that of the local oscillator $\Theta(\mathbf{k}) = \Gamma(\mathbf{k})$, then $U = V = E_{qq} = B_{qq} = 0$, and the expression for the separated state in Eq. (82) would become

$$W_{sv}[\beta](\alpha_0) = 2\exp\left(-2|\alpha_0|^2 g_A - \alpha_0^{*2} g_B - \alpha_0^2 g_B^*\right)$$
$$\times \mathcal{N}_0 \exp\left(-2\beta^* \diamond \beta\right). \quad (107)$$

As a result, the β-dependent part is just a vacuum state, so that after tracing over β, we would recover the same expression as for the naive case given by Eq. (80).

On the other hand, if $\Theta(\mathbf{k}) = \mu\Gamma(\mathbf{k}) + \nu\Lambda(\mathbf{k})$, where $|\mu|^2 + |\nu|^2 = 1$, $\Gamma^* \diamond \Lambda = P \diamond \Lambda = 0$ and $Q \diamond \Lambda = \Lambda$, then the coefficients in Eq. (81) and the kernels in Eq. (83) would become

$$g_E = 2\sinh^2\left(\frac{1}{2}\Xi\right)|\mu|^2, \quad g_B = \sinh(\Xi)\mu^2,$$

$$E_{qq} = 2\sinh^2\left(\frac{1}{2}\Xi\right)|\nu|^2\Lambda\Lambda^*, \quad B_{qq} = \sinh(\Xi)\nu^2\Lambda\Lambda. \quad (108)$$

Moreover,

$$E \diamond \Gamma = 2\sinh^2\left(\frac{1}{2}\Xi\right)(|\mu|^2\Gamma + \mu^*\nu\Lambda),$$

$$B \diamond \Gamma^* = \sinh(\Xi)(\mu^2\Gamma + \nu\mu\Lambda). \quad (109)$$

Hence,

$$U = 2\sinh^2\left(\frac{1}{2}\Xi\right)\nu\mu^*\Lambda, \quad V = \sinh(\Xi)\nu\mu\Lambda,$$

$$\psi = \left[2\sinh^2\left(\frac{1}{2}\Xi\right)\mu^*\alpha_0 + \sinh(\Xi)\mu\alpha_0^*\right]\nu\Lambda. \quad (110)$$
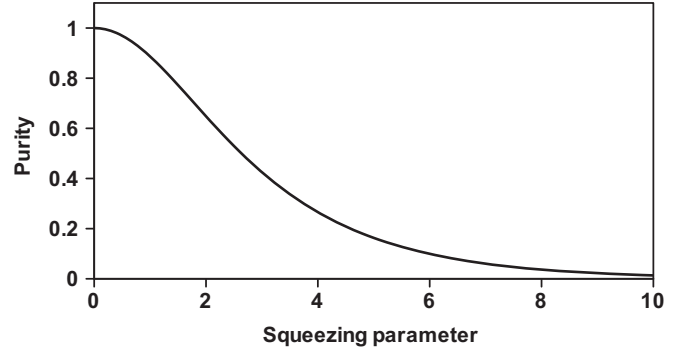

FIG. 3. Purity of the observed single-mode squeezed vacuum state as a function of the squeezing parameter for $|\mu| = \frac{1}{2}$.

With the aid of these quantities and the expressions in Eqs. (90) and (92), we can determine the expression for the observed Wigner function. It reads

$$W_{sv}(\alpha) = \frac{2}{\sqrt{1 + 4|\mu|^2|\nu|^2\sinh^2\left(\frac{1}{2}\Xi\right)}}$$

$$\times \exp\left[-\frac{2|\alpha|^2 + 4|\alpha|^2|\mu|^2\sinh^2\left(\frac{1}{2}\Xi\right)}{1 + 4|\mu|^2|\nu|^2\sinh^2\left(\frac{1}{2}\Xi\right)}\right.$$

$$\left. - \frac{\alpha^{*2}\mu^2\sinh(\Xi) + \alpha^2\mu^{*2}\sinh(\Xi)}{1 + 4|\mu|^2|\nu|^2\sinh^2\left(\frac{1}{2}\Xi\right)}\right]. \quad (111)$$

For $\mu = 1$, the expression becomes equivalent to Eq. (80), and for $\mu = 0$, it becomes that of a vacuum state.

In general Eq. (111) represents a mixed state, with

$$\text{purity} = [1 + 4|\mu|^2|\nu|^2\sinh^2\left(\tfrac{1}{2}\Xi\right)]^{-1/2}. \quad (112)$$

The largest amount of mixing is obtained for $|\mu|^2 = \frac{1}{2}$. The purity for this case is plotted in Fig. 3 as a function of the squeezing parameter.

The amount of squeezing is also diminished by μ. Along the squeezed direction, the standard deviation is

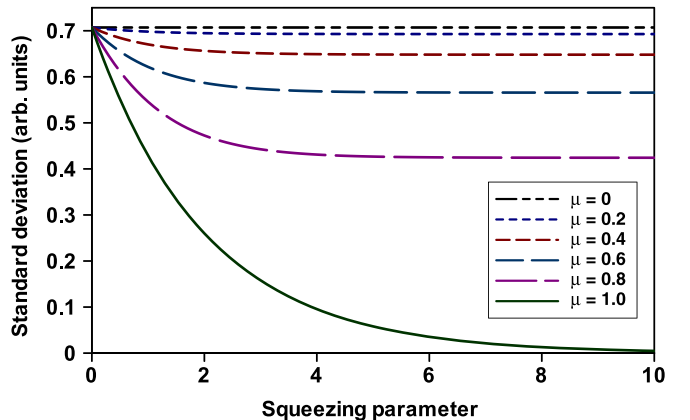$$\sigma_{\min} = \frac{1}{\sqrt{2}}[1 - |\mu|^2 + |\mu|^2\exp(-\Xi)]^{1/2}. \quad (113)$$

FIG. 4. Minimum standard deviation of the observed single-mode squeezed vacuum state as a function of the squeezing parameter for different values of $|\mu|$.

We plot the standard deviation along the squeezed direction in Fig. 4 as a function of the squeezing parameter for different values of $|\mu|$.

IX. CONCLUSIONS

Several observations follow from the analyses provided above. The homodyne tomography process produce some effects that are independent of the states and others that are state-dependent. The state-independent effects include scaling, a finite resolution, and undesirable artifacts. The state-dependent effects are related to the spatiotemporal properties of the state. In general, we see that, unless the input state is parametrized by a single parameter function and both the modes of the local oscillator and the detection system match this parameter function exactly, which assumes *a priori* knowledge of the state's parameter function, the homodyne tomography process produces observed Wigner functions that are distorted.

The main experimental conditions that influence the distortions are those associated with the local oscillator and the detection process. The local oscillator is usually parametrized by a single mode, which determines the spatiotemporal properties of the observed Wigner function. The rest of the spatiotemporal degrees of freedom of the input state are traced out and this trace process can affect the observed Wigner function. The optical power of the local oscillator plays an important role in the process. It sets a boundary for the characteristic function of the state outside of which the characteristic function is set equal to zero. Unless the characteristic function lies inside the boundary, it would be distorted due to clipping. On the phase space, the power (or average number of photons) of the local oscillator determines the resolution of the observed Wigner function. More powerful local oscillators produce better resolution. If the average number of photons in the local oscillator is comparable to those of the state being measured, the resolution would be on the order of the minimum uncertainty area. The effect of the finite resolution is a broadening of the observed Wigner function, which implies that it is rendered as a mixed state.

Provided that the efficiency of the detection process is the same for all photons, regardless of their spatiotemporal degrees of freedom, it only causes a global scaling of the observed Wigner function. Since the homodyne tomography process does not measure the state directly, but instead measures a cross-correlation distribution from which the observed Wigner function is computed, the efficiency does not appear as a probability in the mixture. Instead, our analysis shows that it produces a scaling of the coordinates. This scaling effect can be readily removed by rescaling the phase-space coordinates, provided that the efficiency is known. In those cases where the detection efficiency depends on the spatiotemporal degrees of freedom of the photons, such as would be determined by the overlap with the mode of a single-mode detector, it contributes to the distortion of the observed Wigner function. If the detector can observe photons that are not related to the mode of the local oscillator, it will produce an artifact at the origin of phase space, which would overlap with the Wigner function of a state located at the origin. To avoid such a situation, a single-mode detection system needs to be used where the detector mode is the same as that of the local oscillator.

Some distortions are associated with the loss of purity in the observed Wigner function, even if the state that is being measured is pure and does not suffer a loss of photons. There are different mechanisms responsible for this effect. For a displaced state, such as a coherent state, the observed Wigner function after scaling corrections generally has an increased width, representing a loss of purity. This increase in width is caused by the finite resolution of the intrinsic kernel function of the homodyning process and is not due to a loss of photons. It is proportional to the average number of photons in the state and inversely proportional to the average number of photons in the local oscillator. Even if $\eta = 0$, i.e., without losses in the process, the observed Wigner function is still rendered as a mixed state. Therefore, a local oscillator with a larger optical power will produce an observed Wigner function with a better purity. When the state is located at the origin and is not displaced, the contribution to the loss of purity due to the intrinsic kernel function of the homodyning process is negligible for a suitably large average number of photons in the local oscillator, with the possible exception of severely squeezed states.

However, there are other ways in which states that are located at the origin can lose purity. These cases are related to the properties of the states themselves and result from the trace that removes the degrees of freedom not related to those of the local oscillator and the detection system. If the state is not parametrized by a single parameter function, such as squeezed states, or if its parameter function does not match the mode function of the local oscillator and the detection system, then the trace causes contributions to the observed Wigner function that distort it and contribute to a loss of purity due to the implied loss of photons. The reason can be found in the fact that the spatiotemporal degrees of freedom that are associated with the mode of the local oscillator and the detection system could be entangled with those that are traced out. As a result, the observed Wigner function becomes that of a mixed state. The distortions can also take on other forms. For instance, in the case of a squeezed state, it can reduce to amount of squeezing in the state.

The analysis of the homodyne tomography process with the Wigner functional approach reveals an important aspect of quantum optical states. The marginal distributions that are obtained by integrating the observed Wigner function along one direction are always non-negative. It indicates that the homodyning process always produces observed Wigner functions with valid marginal distributions. However, the input state is represented by a Wigner functional on an infinite-dimensional functional phase space. As a result, the observed Wigner function requires that all the unobserved spatiotemporal degrees of freedom are traced out. This process plays an important role in those cases where the Wigner functional is negative in some regions, such as Fock states and photon-subtracted or photon-added states [26,27]. In a practical scenario, the parameter function that parametrizes a state would not be known before hand, and it would therefore not be possible to match it to the mode of the local oscillator and the detection system. Without the contribution of the trace over the unobserved spatiotemporal degrees of freedom, these negative

regions would not be filled up when the marginal distributions are computed from the observed Wigner function. Therefore, in such practical cases, the trace process may affect those parts of the Wigner functional that become part of the observed Wigner function—those degrees of freedom that are traced out may contribute to the observed Wigner function and are not simply discarded.

APPENDIX: DERIVATIONS OF GENERATING FUNCTIONS

Using the coherent-state-assisted approach (see Appendix B of Ref. [19]), we derive a generating function for the Wigner functionals of single-mode Fock states. The coherent-state-assisted approach produces the Wigner functional of an operator $\hat{A}$ with the aid of

$$
\begin{aligned}
W_{\hat{A}}[\alpha] = \mathcal{N}_0 \int \exp \Bigg(&-2\alpha^* \diamond \alpha + 2\alpha^* \diamond \alpha_1 + 2\alpha_2^* \diamond \alpha \\
&-\frac{1}{2}\alpha_1^* \diamond \alpha_1 - \frac{1}{2}\alpha_2^* \diamond \alpha_2 - \alpha_2^* \diamond \alpha_1 \Bigg) \\
&\times \langle \alpha_1 | \hat{A} | \alpha_2 \rangle \, \mathcal{D}^{\circ}[\alpha_1, \alpha_2].
\end{aligned} \tag{A1}
$$

It requires the functional integrations over two field variables α_1 and α_2.

The single-mode Fock states are defined as

$$
|n_F\rangle = \frac{1}{\sqrt{n!}}\left(\hat{a}_F^{\dagger}\right)^n |\text{vac}\rangle, \quad \langle n_F | = \frac{1}{\sqrt{n!}}\langle \text{vac} | (\hat{a}_F)^n, \tag{A2}
$$

in terms of single-mode ladder operators, given by

$$
\begin{aligned}
\hat{a}_F^{\dagger} &= \sum_s \int \hat{a}_s^{\dagger}(\mathbf{k}) F_s(\mathbf{k}) \frac{d^3 k}{(2\pi)^3 \omega} \equiv \hat{a}^{\dagger} \diamond F, \\
\hat{a}_F &= \sum_s \int F_s^*(\mathbf{k}) \hat{a}_s(\mathbf{k}) \frac{d^3 k}{(2\pi)^3 \omega} \equiv F^* \diamond \hat{a}.
\end{aligned} \tag{A3}
$$

Here, $F_s(\mathbf{k})$ is the angular spectrum of the mode that parametrizes the states.

The density operator of such a Fock state is overlapped on either side by two different coherent states

$$
\begin{aligned}
\langle \alpha_1 | n_F \rangle \langle n_F | \alpha_2 \rangle = \exp\left(-\frac{1}{2}\|\alpha_1\|^2 - \frac{1}{2}\|\alpha_2\|^2\right) \\
\times \frac{1}{n!}(\alpha_1^* \diamond F F^* \diamond \alpha_2)^n,
\end{aligned} \tag{A4}
$$

where $\|\alpha_n\|^2 = \alpha_n^* \diamond \alpha_n$. It is converted to a generating function as follows:

$$
\begin{aligned}
\mathcal{K} &= \sum_n J^n \langle \alpha_1 | n_F \rangle \langle n_F | \alpha_2 \rangle \\
&= \exp\left(-\frac{1}{2}\|\alpha_1\|^2 - \frac{1}{2}\|\alpha_2\|^2 + J\alpha_1^* \diamond F F^* \diamond \alpha_2\right), \tag{A5}
\end{aligned}
$$

where J is the generating parameter. The overlap is recovered by evaluating

$$
\langle \alpha_1 | n_F \rangle \langle n_F | \alpha_2 \rangle = \frac{1}{n!} \partial_J^n \mathcal{K} \bigg|_{J=0}. \tag{A6}
$$

Substituting $\langle \alpha_1 | \hat{A} | \alpha_2 \rangle \to \mathcal{K}$ into (A1), we obtain a generating function for the Wigner functionals of the single-mode Fock states. After performing the functional integrations over α_1 and α_2, we obtain an expression that contains an inverse and a determinant. Thanks to the single-mode property, they can be simplified as

$$
\begin{aligned}
(\mathbf{1} + JFF^*)^{-1} &= \mathbf{1} - \frac{J}{1+J}FF^*, \\
\det\{\mathbf{1} + JFF^*\} &= 1 + J, \tag{A7}
\end{aligned}
$$

leading to an expression of the generating function for the Wigner functionals of the single-mode Fock states that reads

$$
\mathcal{W}_F = \frac{\mathcal{N}_0}{1+J} \exp\left(-2\|\alpha\|^2 + \frac{4J\alpha^* \diamond FF^* \diamond \alpha}{1+J}\right). \tag{A8}
$$

The density operator for an n-photon Fock state represents a projection operator for n photons. In the case of a single-mode Fock state, the projection operator also imposes a modal restriction. To generalize the spatiotemporal degrees of freedom in such projection operators, we replace the mode product $F(\mathbf{k}_1)F^*(\mathbf{k}_2)$ in the expression of the generating function by a general kernel $P(\mathbf{k}_1, \mathbf{k}_2)$. In this case, the determinant becomes

$$
\det\{\mathbf{1} + JP\} = (1+J)^{\text{tr}\{P\}}. \tag{A9}
$$

The trace over the kernel $\text{tr}\{P\}$ counts the number of degrees of freedom that can pass through the kernel. For example, if the kernel can be diagonalized in terms of N orthogonal functions:

$$
P(\mathbf{k}_1, \mathbf{k}_2) = \sum_{n=1}^{N} F_n(\mathbf{k}_1)F_n^*(\mathbf{k}_2), \tag{A10}
$$

then $\text{tr}\{P\} = N$. For $P = \mathbf{1}$, the summation over the number of modes needs to be extended to infinity to include all the elements of a complete basis. As a result, the trace over P produces the number of degrees of freedom of the entire phase space, which we represent by Ω.

However, an n-photon state may contain photons with different spatiotemporal degrees of freedom. Hence, we need to trace out those photons that do not have the correct spatiotemporal degrees of freedom to be allowed through by P. It can be done by considering another generating function with a kernel $Q = \mathbf{1} - P$ and with a different generating parameter. Then the combined generating function for both these kernels

is used to evaluate the trace over the other photons. It is easily done by setting the other generating parameter equal to 1. The resulting generating function for the projection operators is then given by

$$\mathcal{W}_P = \left(\frac{2}{1+J}\right)^{\mathrm{tr}\{P\}} \exp\left(-2\frac{1-J}{1+J}\alpha^* \diamond P \diamond \alpha\right). \quad \text{(A11)}$$

This generating function can be used to model a photon-number resolving detector where the physical properties of the detector is modeled by the kernel function $P = D$. For $D = FF^*$, the detector kernel represents a single-mode detector and $\mathrm{tr}\{D\} = F^* \diamond F = 1$. For a bucket detector on the other hand, the detector kernel is proportional to the identify. Then $\mathrm{tr}\{D\} = \Omega$.

[1] A. I. Lvovsky and M. G. Raymer, Continuous-variable optical quantum-state tomography, Rev. Mod. Phys. **81**, 299 (2009).

[2] D. T. Smithey, M. Beck, M. G. Raymer, and A. Faridani, Measurement of the Wigner Distribution and the Density Matrix of a Light Mode Using Optical Homodyne Tomography: Application to Squeezed States and the Vacuum, Phys. Rev. Lett. **70**, 1244 (1993).

[3] G. Breitenbach, S. Schiller, and J. Mlynek, Measurement of the quantum states of squeezed light, Nature (London) **387**, 471 (1997).

[4] A. I. Lvovsky, H. Hansen, T. Aichele, O. Benson, J. Mlynek, and S. Schiller, Quantum State Reconstruction of the Single-Photon Fock State, Phys. Rev. Lett. **87**, 050402 (2001).

[5] A. Zavatta, S. Viciani, and M. Bellini, Tomographic reconstruction of the single-photon Fock state by high-frequency homodyne detection, Phys. Rev. A **70**, 053821 (2004).

[6] A. Ourjoumtsev, R. Tualle-Brouri, and P. Grangier, Quantum Homodyne Tomography of a Two-Photon Fock State, Phys. Rev. Lett. **96**, 213601 (2006).

[7] A. Zavatta, S. Viciani, and M. Bellini, Quantum-to-classical transition with single-photon-added coherent states of light, Science **306**, 660 (2004).

[8] A. Zavatta, V. Parigi, and M. Bellini, Experimental nonclassicality of single-photon-added thermal light states, Phys. Rev. A **75**, 052106 (2007).

[9] A. Ourjoumtsev, R. Tualle-Brouri, J. Laurat, and P. Grangier, Generating optical Schrödinger kittens for quantum information processing, Science **312**, 83 (2006).

[10] A. Ourjoumtsev, H. Jeong, R. Tualle-Brouri, and P. Grangier, Generation of optical "Schrödinger cats" from photon number states, Nature (London) **448**, 784 (2007).

[11] K. Vogel and H. Risken, Determination of quasiprobability distributions in terms of probability distributions for the rotated quadrature phase, Phys. Rev. A **40**, 2847 (1989).

[12] U. Leonhardt and H. Paul, Realistic optical homodyne measurements and quasiprobability distributions, Phys. Rev. A **48**, 4598 (1993).

[13] H. Kühn, D.-G. Welsch, and W. Vogel, Determination of density matrices from field distributions and quasiprobabilities, J. Mod. Opt. **41**, 1607 (1994).

[14] Y. Shaked, Y. Michael, R. Z. Vered, L. Bello, M. Rosenbluh, and A. Pe'er, Lifting the bandwidth limit of optical homodyne measurement with broadband parametric amplification, Nat. Commun. **9**, 609 (2018).

[15] M. G. Raymer, J. Cooper, H. J. Carmichael, M. Beck, and D. T. Smithey, Ultrafast measurement of optical-field statistics by dc-balanced homodyne detection, J. Opt. Soc. Am. B **12**, 1801 (1995).

[16] J. Appel, D. Hoffman, E. Figueroa, and A. I. Lvovsky, Electronic noise in optical homodyne tomography, Phys. Rev. A **75**, 035802 (2007).

[17] F. S. Roux, Combining spatiotemporal and particle-number degrees of freedom, Phys. Rev. A **98**, 043841 (2018).

[18] F. S. Roux, Spatiotemporal effects on squeezing measurements, Phys. Rev. A **103**, 013701 (2021).

[19] F. S. Roux, Parametric down-conversion beyond the semiclassical approximation, Phys. Rev. Research **2**, 033398 (2020).

[20] F. S. Roux, Stimulated parametric down-conversion for spatiotemporal metrology, Phys. Rev. A **104**, 043514 (2021).

[21] F. S. Roux, Toolbox for non-classical state calculations, J. Opt. (Bristol, U.K.) **23**, 125201 (2021).

[22] M. G. Paris, Quantum state measurement by realistic heterodyne detection, Phys. Rev. A **53**, 2658 (1996).

[23] U. Chabaud, G. Roeland, M. Walschaers, F. Grosshans, V. Parigi, D. Markham, and N. Treps, Certification of non-Gaussian states with operational measurements, PRX Quantum **2**, 020333 (2021).

[24] H. Vahlbruch, M. Mehmet, K. Danzmann, and R. Schnabel, Detection of 15 dB Squeezed States of Light and their Application for the Absolute Calibration of Photoelectric Quantum Efficiency, Phys. Rev. Lett. **117**, 110801 (2016).

[25] C. K. Law and J. H. Eberly, Analysis and Interpretation of High Transverse Entanglement in Optical Parametric Down Conversion, Phys. Rev. Lett. **92**, 127903 (2004).

[26] M. Walschaers, V. Parigi, and N. Treps, Practical framework for conditional non-Gaussian quantum state preparation, PRX Quantum **1**, 020305 (2020).

[27] A. I. Lvovsky, P. Grangier, A. Ourjoumtsev, V. Parigi, M. Sasaki, and R. Tualle-Brouri, Production and applications of non-gaussian quantum states of light, arXiv:2006.16985.